Int. J. Electrochem. Sci., 10 **(2015)** 5513 - 5520

International Journal of
ELECTROCHEMICAL
SCIENCE
www.electrochemsci.org

Electron Lifetimes in Hierarchically Structured Photoelectrodes Biotemplated from Butterfly Wings for Dye-Sensitized Solar Cells

Jung-Hun Kim[1], *Tae Young Kim*[2], *Kyung Hee Park*[3], *Jae-Wook Lee*[1,*]

[1]Department of Chemical and Biochemical Engineering, Chosun University, Gwangju 501-759, Republic of Korea
[2]Department of Environmental Engineering, Chonnam National University, Gwangju 500-757, Republic of Korea
[3]The Research Institute of Advanced Engineering Technology, Chosun University, Gwangju 501-759, Republic of Korea
[*]E-mail: jwlee@chosunn.ac.kr

Received: 25 March 2015 / *Accepted:* 8 May 2015 / *Published:* 27 May 2015

Hierarchical structures for TiO_2 photoelectrodes, biotemplated from *Parpilio paris* butterfly wings, were synthesized and applied to dye-sensitized solar cells (DSSCs). The synthesized samples were characterized by field emission scanning electron microscopy (FE-SEM), X-ray diffraction (XRD), and electrochemical impedance spectroscopy (EIS). The adsorption kinetics of N719 dye molecules on thin TiO_2 films was measured and interpreted using a pseudo-second order model. Open-circuit voltage-decay (OCVD) measurements were employed to investigate the recombination kinetics of the fine hierarchical structure. The electron lifetimes, determined by EIS, in films prepared with TiO_2 nanoparticles only or with a mixture of TiO_2 nanoparticles and hierarchical butterfly-wing-templated structures were respectively 6.1 and 7.4 ms, with photovoltaic conversion efficiencies of 3.48 and 4.32%, respectively. The morphology of films therefore plays an important role in their light harvesting behavior and hierachical structures lead to increased absorption.

Keywords: Electron Lifetime, Hierarchical Structure, Butterfly Wing, Dye-Sensitized solar Cell

1. INTRODUCTION

Dye-sensitized solar cells (DSSCs) were first reported by Gratzel in 1991 [1]. The initial design consisted of a dye-adsorbed mesoporous titania film filled with iodide/triiodide redox electrolyte and a Pt counter photoanode. Much effort has subsequently been devoted to improving the photovoltaic conversion efficiency. Theoretically, a perfect photoelectrode for DSSCs must provide fast electron injection and separation, fast electron transport, slow electron recombination, a high surface area, and excellent light collection [2]. The photonic structures in butterfly wings have been found to be promising in infrared detectors, photo trappers, and flat-panel displays [3]. Recently, a novel photoelectrode structure biotemplated from a butterfly wing has been developed to improve the light absorbing performance of DSSCs.

Liu et al. proposed a facile one-step approach for the replication of butterfly wings in TiO_2, with the resulting structures containing ordered mesopores [4]. Han et al. reported light trapping effects in the wing scales of the butterfly *Papilio peranthus*. A complex functional structure is formed by a variety of monolayer films with different refractive indexes and thicknesses. Interference between neighboring ridges in the multilayer film structure leads to a light trapping effect [5]. Zang et al. synthesized a novel photoanode templated from butterfly wing scales, with a quasi-honeycomb structure composed of shallow concavities and cross-ribbing. The quasi-honeycomb-structured TiO_2 replica photoanode was found to have a higher surface area and increased light absorbance, both of which are advantageous in terms of light harvesting efficiency and dye sorption [6]. A number of other studies have focused mainly on structural properties [7–9]. Unfortunately, no systematic study has been performed so far of the influence of dye sorption and electron lifetime on the photovoltaic conversion efficiency of DSSCs. In this work therefore, TiO_2 photoelectrodes were biotemplated from a *Parpilio paris* butterfly wing and their fine hierarchical structure was characterized by field emission scanning electron microscopy (FE-SEM), X-ray diffraction (XRD), and electrochemical impedance spectroscopy (EIS). The adsorption kinetics of N719 dye molecules on thin TiO_2 films was measured and analyzed using a pseudo-second order model. The electron lifetime in hierarchical TiO_2 photoelectrodes was determined from open-circuit-voltage-decay (OCVD) curves.

2. EXPERIMENTAL

The wings of the butterfly *Papilio paris* were used as biotemplates in our work. Analytical grade reagents HCl, NaOH, poly(ethylene glycol)-poly(propylene glycol)-poly(ethylene glycol) (PEG-PPG-PEG), and $TiCl_4$ were provided by Sigma-Aldrich. The butterfly wings were pretreated in 2M HCl and 2M NaOH to remove salts and proteins. The pretreated wings were then carefully immersed in a solution of ethanol/PEG-PPG-PEG, 3.7 mmol/L $TiCl_4$ was separately added, and the mixture was ultra-sonicated at room temperature using a high-intensity ultrasonic probe. The sonicated butterfly wings were washed five times with ethanol, dried in air, and then calcined at 450 °C for 3 h. The chitin substrates and surfactant were removed by reaction with the air. Then, metal oxide with the form of the ceramic butterfly wings is obtained. The resulting replicas are named "butterfly wings TiO_2" (BF-TiO_2) in the following. To make the BF-TiO_2 paste, 10 wt.% BF-TiO_2 was added to commercial TiO_2 nanoparticle paste (NP-TiO_2) and mixed for 1 h. The prepared pastes were coated on fluorine-doped tin oxide (FTO) glass by squeeze printing and then sintered at 450 °C for 30 min. The prepared NP and BF electrodes were immersed overnight (ca. 24 h) in a 5×10^{-4} mol/L ethanol solution of $Ru(dcbpy)_2(NCS)_2$ (N719, Solaronix), rinsed with anhydrous ethanol, and dried. TiO_2 film, about 7 μm thick, was deposited on a 0.25 cm^2 FTO glass substrate. The electrode, electrolyte, and DSSCs were assembled as described in our previous reports [10]. The prepared samples were analyzed using an ultraviolet-visible (UV-Vis) spectrophotometer (UV-1601A, Shimadzu, Japan) and an electrochemical workstation (CHI660A, CH Instruments, USA). Photovoltaic properties were investigated by measuring J-V characteristics under 200 W white light irradiation from a xenon lamp (McScience, Korea).

3. RESULTS AND DISCUSSION

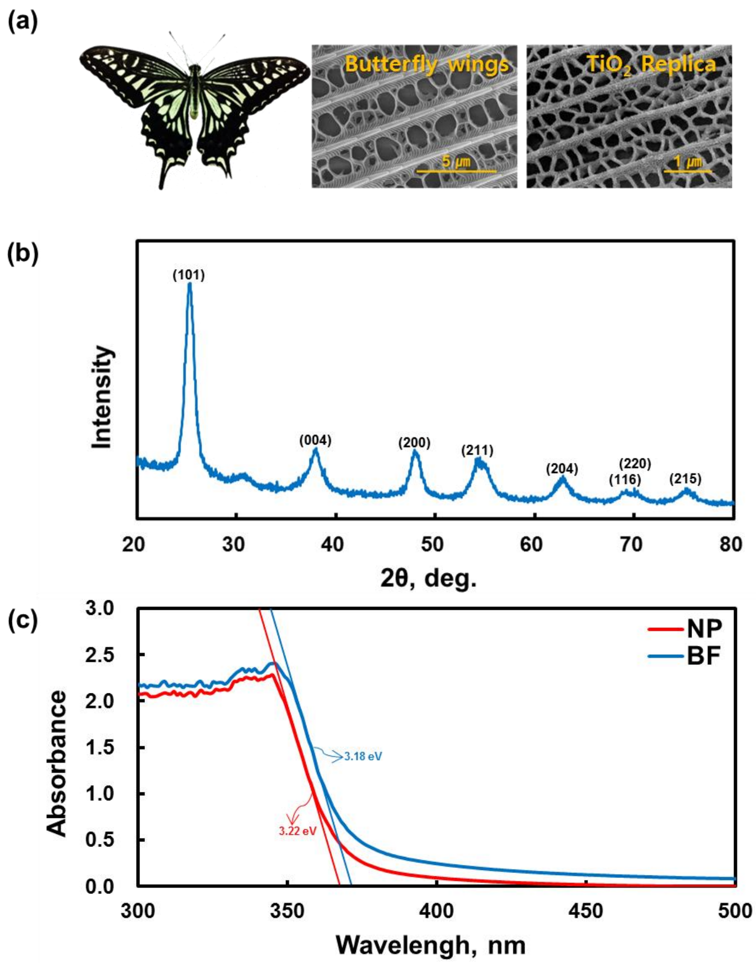

Figure 1. (a) FE-SEM images (b) XRD patterns and (c) UV-Vis absorption spectra obtained from NP-TiO_2 and BF-TiO_2 cells.

Fig. 1(a) shows the wing architecture of *Papilio paris*, a species of butterfly found in Asia, and its TiO_2 replica. The scales in the original butterfly wing have parallel ridges spaced several microns apart and aligned lengthwise. The lamellae (ridges) are hollow and comprise cross-ribs on the bottom surface. The ridges are composed of nano-scale ribs (~10 nm in width) approximately 50 nm apart. The fine microstructural details of the original butterfly wing scales are still observed after calcination in the BF-TiO_2 samples. However, the inter-lamellae spacing has shrunk by ~48% to approximately 0.56 µm, due to the elevated calcination temperature.

Fig. 1(b) shows XRD patterns obtained from BF-TiO_2 samples calcined at 450 °C. Eight peaks are observed, at 2θ values of 25.2, 37.8, 48.0, 55.0, 62.6, 68.7, 70.3, and 75.0° corresponding to the (101), (004), (200), (211), (204), (116), (220), and (215) crystal planes of anatase TiO_2 (JCPDS no. 21-1272). The average crystallite size of BF-TiO_2 is around 12.1 nm, as calculated using Scherrer's formula from the XRD patterns:

$$D = \frac{k\lambda}{\beta \cos\theta} \qquad (1)$$

where D is the crystallite size, λ is the wavelength of the X-rays, β is the width of the diffraction line measured at half the maximum intensity, and θ is the corresponding angle.

The light harvesting properties of the samples were examined using absorbance spectroscopy. Fig. 1(c) shows the optical properties of BF-TiO_2 and NP-TiO_2 films. The UV-Vis curve for BF-TiO_2 is redshifted compared with the one measured for the NP-TiO_2 films. In addition, the BF-TiO_2 film strongly absorbs visible wavelengths between 400 and 500 nm. The absorption edge for the two samples was determined using the following equation [11]:

$$E_g = {}^{1239.8}/_{\lambda} \qquad (2)$$

where E_g is the band-gap (eV) of the sample, and λ (nm) is the wavelength of the onset of absorption. The energy band gaps for the NP-TiO_2 and BF-TiO_2 films are thereby calculated to be 3.22 and 3.18 eV, respectively. The BF-TiO_2 sample has a greater absorbance than NP-TiO_2, suggesting that film morphology plays an important role in light harvesting and that hierachical structures have high absorption properties.

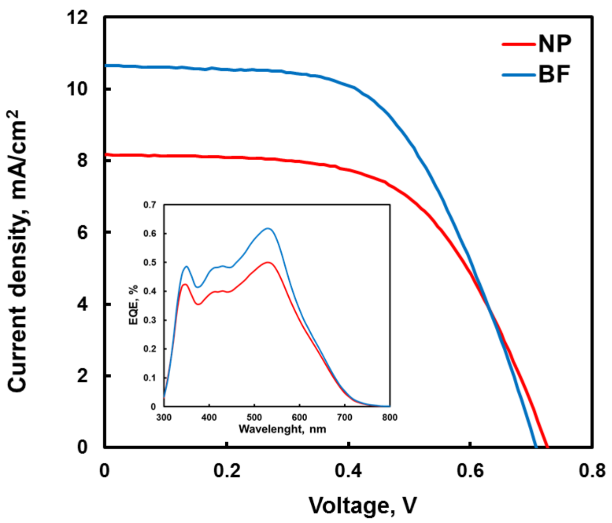

Figure 2. Photocurrent-voltage (J-V) and (inset) incident photon to current conversion efficiency curves for NP-TiO_2 and BF-TiO_2 cells.

The incident photon to current conversion efficiency (IPCE) spectra obtained from the NP-TiO_2 and BF-TiO_2 samples are shown in Fig. 2. The peak efficiency at 530 nm corresponds to the maximum absorption wavelength of the N719 dye. For all wavelengths, the external quantum efficiency is higher for the BF-TiO_2 than for NP-TiO_2 electrode, which is consistent with the J_{sc} values obtained by photocurrent-voltage measurements (see below). The IPCE peak height at 530 nm for the BF-TiO_2 electrode is 61.8%, which is much higher than the value of 50% obtained with the NP-TiO_2 electrode. Fig. 2 shows the photocurrent-voltage curves obtained for the NP-TiO_2 and BF-TiO_2 photoelectrodes. The BF cell achieved a short-circuit current density (J_{sc}) of 10.66 mA/cm^2 and an energy conversion efficiency (η) of 4.32% (Fig. 5 and Table 1). In comparison, the DSSC made using the NP-TiO_2 had J_{sc} and η values of 8.17 mA/cm^2 and 3.48%, respectively. These results indicate that the 24% improvement in η results mainly from the 30% increase in J_{sc}. The increase in the latter is probably due to the improved light scattering and dye uptake afforded by the BF-TiO_2.

Table 1. Photocurrent-voltage (J-V) characteristics of NP-TiO_2 and BF-TiO_2 cells

Samples	J_{sc} [mA/cm^2]	V_{oc} [V]	Fill Factor [%]	Efficiency [%]
NP-TiO_2	8.17	0.73	58.6	3.48
BF-TiO_2	10.66	0.71	57.3	4.32

The photovoltaic conversion efficiency of materials is known to be highly dependent on their adsorption properties.

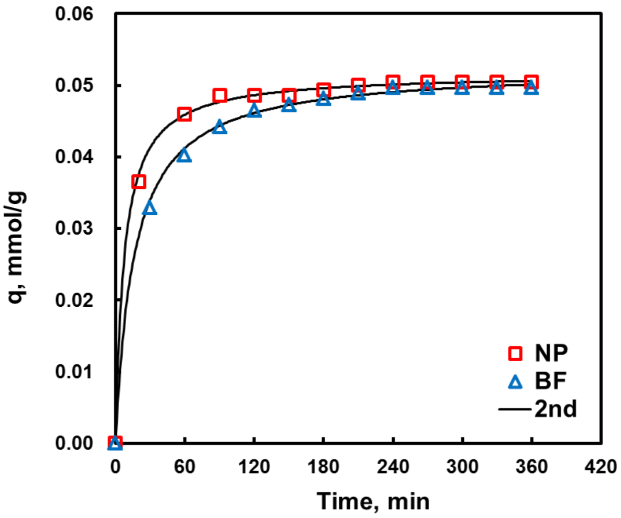

Figure 3. Adsorption kinetics of N719 dye on NP-TiO_2 and BF-TiO_2 cells.

Adsorption kinetics can be used to understand the sorption mechanism on mesoporous TiO_2 thin films. Fig. 3 shows the adsorption kinetics of N719 on NP-TiO_2 and BF-TiO_2 thin films obtained in a small-batch adsorption chamber without a desorption step [12]. The parameters obtained from pseudo second-order models of the kinetics of N719 adsorption on the NP-TiO_2 and BF-TiO_2 thin films are listed in Table 2. The models fit the experimental data very well ($R^2 > 1.0$). For NP-TiO_2 and BF-TiO_2, the second-order rate constants are respectively 2.57 and 1.18 g/(mol·min), with the same q_e, 0.052 mmol/g, for both samples.

Table 2. Kinetic adsorption characteristics of NP-TiO_2 and BF-TiO_2 cells

Samples	k_2 [g/mol·min]	q_e [mmol/g]	R^2
NP-TiO_2	2.57	0.052	1.00
BF-TiO_2	1.18	0.052	1.00

To investigate the recombination kinetics in fine hierarchical structures, open-circuit voltage-decay (OCVD) measurements reported by Zaban and Greenshtein [13] are used. As shown in Fig. 4(a), OCVD measurements were conducted by monitoring the V_{OC} transient during relaxation from an illuminated quasiequilibrium state to the dark equilibrium. The photovoltage decay rate directly related to the electron lifetime by the following expression:

$$\tau_n = \frac{-k_B T}{e}\left[\frac{dV_{oc}}{dt}\right]^{-1} \qquad (3)$$

τ_n is thereby the reciprocal of the derivative of the decay curve normalized by the thermal voltage, $k_B T$ is the thermal energy, e is the elementary charge, and dV_{oc}/dt is the derivative of the open circuit voltage transient. Eq. (3) is obtained based on the assumption that the recombination is linear with a first-order dependence on the electron concentration and that electron recombination occurs only with the electrolyte. Fig. 4(a) shows the OCVD curves measured for NP-TiO_2 and BF-TiO_2 cells. The voltage decay of the BF-TiO_2 cell is slower than the NP-TiO_2. Fig. 4(b) shows the response times obtained by applying Eq. (3) to the data of Fig. 4(a). Electron recombination is slow in both the BF-TiO_2 and NP-TiO_2 cells, allowing them to sustain significant voltages many seconds after the light has been turned off. The τ_n values are much larger in the BF-TiO_2 than in the NP-TiO_2 cell. This result suggests that the recombination of the photogenerated electrons with electrolyte-oxidized species is slower in the BF-TiO_2 electrode. This effect may also explain the higher performance of the BF-TiO_2 DSSC electrode.

To examine the internal resistance and charge-transfer kinetics of the samples, EIS was performed under illumination at an applied bias of V_{OC} with an AC amplitude of 10 mV. Fig. 5(a) shows the Nyquist plots obtained for the NP-TiO_2 and BF-TiO_2 cells. Two well-defined semicircles are charge transfer resistance at the electrolyte–Pt–FTO interface (R_{ct1}) and charge transfer resistance at the TiO_2–dye–electrolyte interface (R_{ct2}). The equivalent-circuit model of the DSSCs is shown in the

Fig. 5(a) inset. The serial resistance (R_s) of the NP-TiO_2 cell is slightly larger than that of the BF-TiO_2 cell, such that the former has a lower fill factor than the latter.

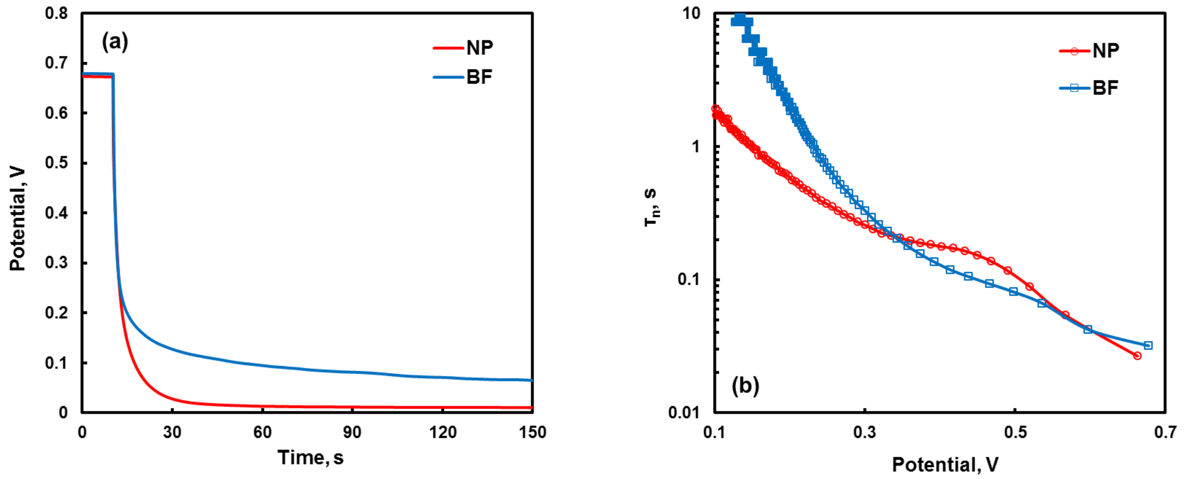

Figure 4. (a) OCVD curves and (b) the corresponding response times for NP-TiO_2 and BF-TiO_2 cells.

The R_{ct1} resistances of the two DSSCs are almost identical, whereas the R_{ct2} resistance of the BF-TiO_2 cell is smaller. For the NP-TiO_2 and BF-TiO_2 cells, R_{ct2} values of about 37.1 Ω and 19.1 Ω are obtained, respectively, by fitting the Nyquist plots to the equivalent circuit mode. These values indicate faster electron transfer in the BF-TiO_2 cell. As supported by the UV-Vis spectra, this can be attributed to more efficient light harvesting.

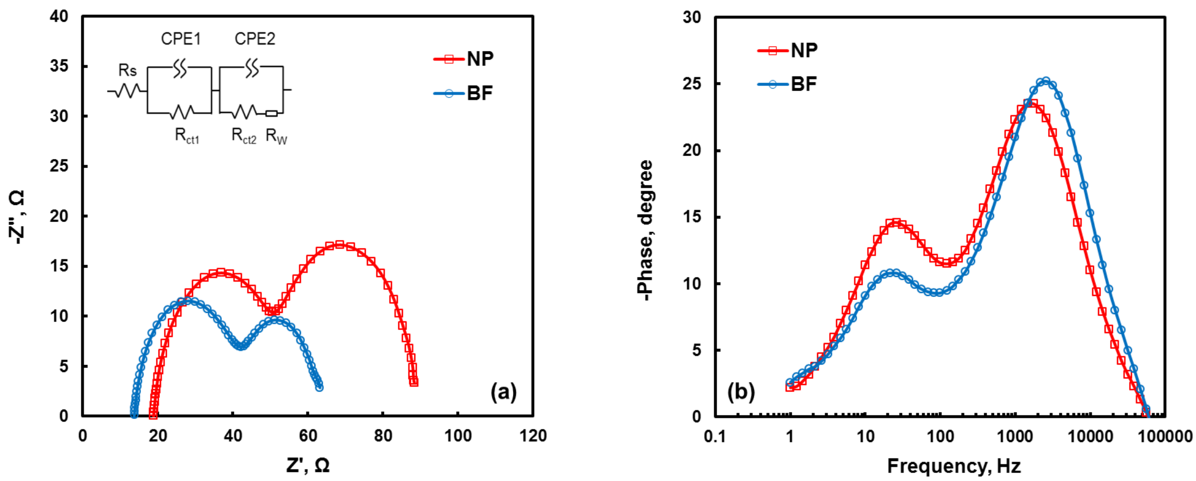

Figure 5. (a) Nyquist plots and (b) Bode phase plots for NP-TiO_2 and BF-TiO_2 cells. The inset in (a) shows the equivalent circuit model of both cells.

The electron lifetime (τ_e) in the TiO_2 films can be obtained from the characteristic angular frequency (ω_{mid}) of the middle frequency (f_{mid}) peak in the Bode phase plots, using the relation of τ_e =

$1/\omega_{mid} = 1/2\pi f_{mid}$. The Bode phase plots for the NP-TiO_2 and BF-TiO_2 cells are shown in Fig. 5(b). The characteristic frequency for the BF-TiO_2 cell is down-shifted by 26.1 Hz with respect to the corresponding peak for the NP-TiO_2 cell. The electron lifetimes for the NP-TiO_2 and BF-TiO_2 cells obtained from these peaks are 6.1 and 7.4 ms, respectively. This result implies that film morphology plays an important role in DSSC electron recombination.

4. CONCLUSIONS

Fine hierarchical TiO_2 structures were successfully synthesized using *Parpilio paris* butterfly wings as biotemplates. The prepared samples have homogeneous pores, ca. 0.1–0.5 nm in size, and large pore volumes and surface areas. The electron lifetimes in NP-TiO_2 and BF-TiO_2 films, determined from EIS measurements, are 6.1 and 7.4 ms, respectively, with photovoltaic conversion efficiencies of 3.48 and 4.32%, respectively. These results show that hierachical structures have an important and positive impact on light absorption and light harvesting properties.

ACKNOWLEDGMENTS
This study was supported by Research Funds from Chosun University, 2013.

References

1. B. O`Regan, M. Gratzel, *Nature*, 353 (1991) 737
2. J. H. Yum, E. Baranoff, S. Wenger, M.K. Nazeeruddin, M. M. Gratzel, *Energy Environ. Sci*, 4 (2011) 842
3. S. Zhu, D. Zang, Z. Chen, J. Gu, W. Li, H. Jiang, G. Zhou, *Nanotechnology*, 20 (2009) 315303
4. X. Liu, S. Zhu, D. Zhang, Z. Chen, *Materials Lett*, 64 (2010) 2745
5. Z, Han, S. Niu, L. Zhang, Z. Liu, L. Ren, *J. Bionic Eng*, 10 (2013) 162
6. W. Zhang, D. Zhang, T. Fan, J. Gu, J. Ding, H. Wang, Q. Guo, H. Ogawa, *Chem. Mater*, 21 (2009) 33
7. C. Yin, S. Zhu, F. Yaom J. Gu, W. Zhang, Z. Cehn, D. Zhang, *J. Nanopart Res.* 15 (2013) 1812
8. L. Ding, H. Zhou, S. Lou, J. Ding, D. Zhang, H. Zhu, T. Fan, Int. *J. Hydrogen Energy*, 38 (2013) 8244.
9. H. Liu, Q. Zhao, H. Zhou, J. Ding, D. Zhang, H. Zhu, T. Fan, *Phys. Chem. Chem. Phys*, 13 (2011) 10872
10. K.H. Park, T.Y. Kim, J.H. Kim, H.J. Kim, C.K. Hong, J.W. Lee, *J. Electrocannal. Chem*, 708 (2013) 39
11. T. Horikawa, M. Katoh, T. Tomida, *Micropor. Mesopor. Mater*, 110 (2008) 397
12. T.Y. Kim, J.W. Lee, E.M. Jin, J. Y. Park, J. H. Kim, K. H. Park, *Measurement*,46 (2013) 1692
13. A. Zaban, M. Greenshtein, *Chem. Phys. Chem*, 4 (2003) 859.